

Optical Trapping of Nanoparticles and Quantum Dots

Poul M. Bendix, Liselotte Jauffred, Kamilla Norregaard, and Lene B. Oddershede

(Invited Paper)

Abstract—Optical manipulation of nanostructures offers new exciting possibilities for building new nano-architectures and for exploring the fundamental interactions between light and nanoparticles. The optical properties of nanostructures differ substantially from those of similar bulk material and exhibit an exquisite sensitivity on nanoparticle shape and composition. The plethora of particles available today expands the possibilities of optical manipulation to include control over particle temperature, luminescence, orientation, and even over the rotational optical momentum transferred to the nanoparticle. Here, we summarize recent experimental advances within optical manipulation of individual nanoparticles and quantum dots with a focus on resonant versus non-resonant trapping, optically induced heating, spherical aberration, and orientation control. Also, we present novel quantitative data on the photonic interaction between gold nanoshells and a focused laser beam. Lastly, promising applications of the biophotonic properties of nanoparticles within nanoscience and biophysics are pointed out.

Index Terms—Optical trapping, dielectric nanoparticles, gold nanoparticles, gold nanorods, gold nanoshells, liposomes, plasmonic tweezers, plasmonic heating, quantum dots, spherical aberration, nanosensor, patterning, DNA hybridization.

I. INTRODUCTION

OPTICAL trapping of nanoparticles is a field that is currently being intensely driven by the desire to achieve precise translation and rotational control over nanostructures. An optically mediated contactless control over nanoparticles offers a unique way to do this and to investigate the physics of single or multiple particles in presence of light without any interfering substrate. This, as well as the recent progress within nanostructure architecture and design, has prompted a significant amount of exploration of how individual nanoparticles, or a collection of particles, interact with resonant or off-resonant light [1]–[5].

Optical confinement of Rayleigh particles, whose linear dimensions are significantly smaller than the trapping wavelength, has been challenging because the trapping force scales with the polarizability of the particle. Therefore, effort has been put into testing nanoparticle materials that have enhanced polarizability [6], [7] and to modify the shape of the trapping beam to

optimize the trapping potential [8]–[10]. A high polarizability of nanomaterials is also associated with high absorption and consequently the irradiated nanoparticle will emit heat to its surroundings [2], [11]–[14]. Although heating is often undesired, irradiation of nanoparticles does offer a unique way to control temperature at the nanoscale with extremely high temperature gradients, an effect which is anticipated to have great potential in photothermal therapies of, e.g., malignant tissue [15]–[17]. Heating generated from irradiation of plasmonic nanoparticles can also be used, e.g., to tune DNA hybridization between nanoparticles containing complementary single stranded DNA [18]. Novel types of nanostructures, like nanorods or nanoshells, can be readily synthesized with plasmonic resonances that can be tuned by changing the particle's aspect ratio (length divided by width) [15] or core-shell ratio [19], respectively. The exact location of the particle's resonance critically influences its interaction with a trapping laser beam [12], [20].

Dielectric and biological nanoparticles are typically less absorptive in particular at near infrared (NIR) wavelengths and consequently higher powers can be used for trapping without extensive heating of the particle [21]–[25]. Manipulation of nano-sized biological constructs such as lipid vesicles [25] offers great potential for probing membrane protein mediated interactions with proteins embedded in their natural environment as is highly relevant, for instance, in the context of SNARE (Soluble NSF Attachment protein Receptor) mediated membrane fusion [26], [27].

Here, we focus on precise optical control and quantitative measurements of individual spherical and rod like nanoparticles made of various materials including metals, semiconductors, and composites. Hence, we mainly focus on optical manipulation by a single tightly focused Gaussian laser beam, but also touch on the exciting progress in development of new optical configurations allowing multiple trapping [28], beam shaping [10], [29], [30] and of plasmonic trapping of nanoparticles [31]–[33].

II. OPTICAL INTERACTIONS

A. Relevant Optical Forces

As the wavelength of visible and NIR light is significantly longer than the typical linear dimension of nanoscopic particles the mechanism of trapping can be most conveniently explained by considering the nanoparticle as an induced point dipole moving in an inhomogeneous electromagnetic field. Such a dipole is affected by a force, \mathbf{F} (the gradient force):

$$\mathbf{F} = \frac{1}{2} |\alpha| \nabla \langle \mathbf{E}^2 \rangle \quad (1)$$

Manuscript received August 1, 2013; revised October 7, 2013; accepted October 15, 2013. This work was supported by Villum Kann Rasmussen Foundation, The Copenhagen University Excellence Program and the Carlsberg Foundation.

The authors are with the Niels Bohr Institute, University of Copenhagen, 2100 Copenhagen, Denmark (e-mail: bendix@nbi.dk; jauffred@nbi.dk; kamilla@nbi.dk; oddershede@nbi.dk).

Color versions of one or more of the figures in this paper are available online at <http://ieeexplore.ieee.org>.

Digital Object Identifier 10.1109/JSTQE.2013.2287094

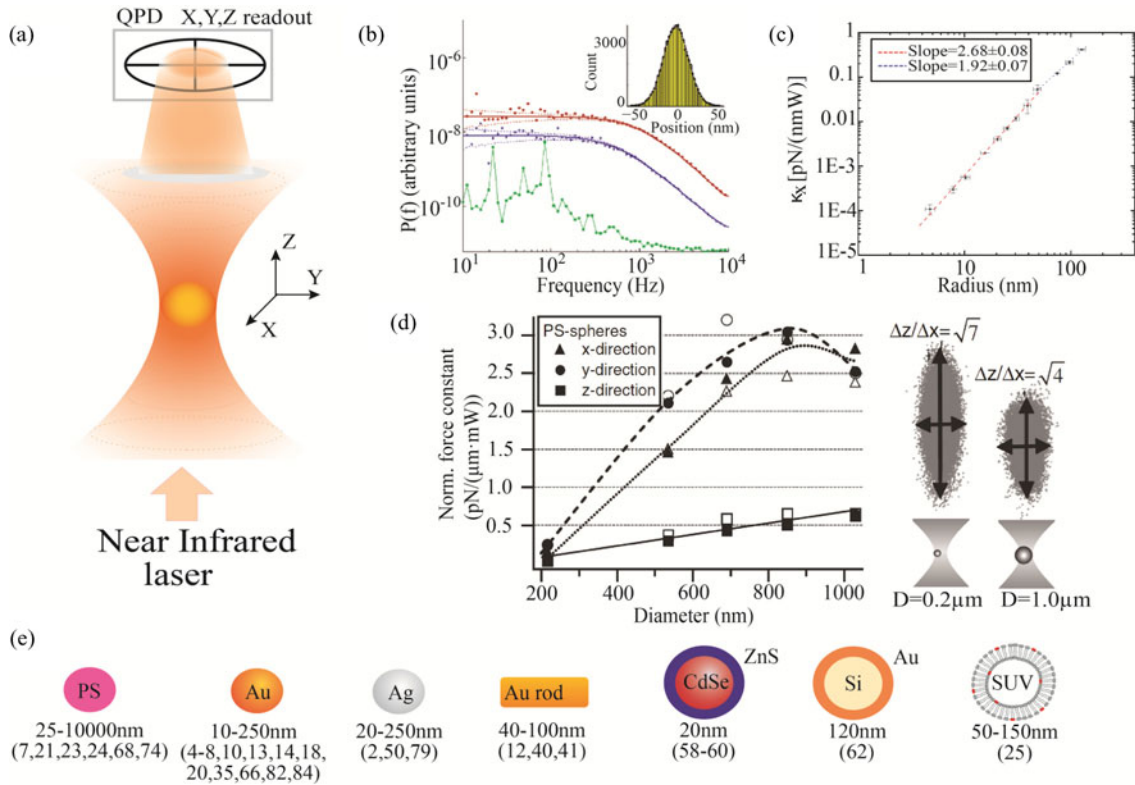


Fig. 1. Optical trapping of nanospheres and quantification of their interaction with the field. (a) Schematic of a single beam optical trap where a NIR laser is focused to a diffraction limited spot. Optical gradient forces attract the nanoparticle to the center of the laser focus. The particle's positions are recorded with nanometer spatial resolution and ~ 100 kHz time resolution by using a quadrant photodiode (QPD) to detect the forward scattered light. (b) Power spectra of the time series for two trapped gold nanoparticles with $d = 30$ nm (blue triangles) and $d = 196$ nm (red circles), respectively. The green squares represent the noise from an empty trap. The inset shows the position histogram of the $d = 196$ nm gold nanoparticle, it has a Gaussian shape because the particle moves in a harmonic potential, reproduced with permission from [6]. (c) Spring constants characterizing the lateral strength of the optical trap while trapping gold nanoparticles of various sizes, reproduced with permission from [8]. (d) Spring constants, and their asymmetry for the translational directions, measured for optical trapping of polystyrene nanoparticles, reproduced with permission from [21]. (e) Overview of different types of nanoparticles individually optically trapped in 3-D together with the corresponding references.

where α is the polarizability of the particle, \mathbf{E} is the electromagnetic field, and the brackets denote time averaging. $|\mathbf{E}^2|$ is proportional to the field intensity and \mathbf{F} points along the gradient of the light intensity (toward increasing intensity). Therefore, in a laser beam tightly focused in three dimensions [as sketched in Fig. 1(a)], a point dipole will be attracted toward the focal spot.

Another important optical force, \mathbf{F}_{rad} , arises from the radiation pressure on the particle when photons become scattered or absorbed at the incident particle surface [34]:

$$\mathbf{F}_{\text{rad}} = \frac{n \langle \mathbf{P} \rangle}{c} C_{\text{ext}} \quad (2)$$

where $\langle \mathbf{P} \rangle$ is the time average of the Poynting vector, n is the index of refraction of the surrounding liquid, and c is the speed of the light. C_{ext} is the extinction cross section which is a sum of the absorption and scattering cross sections:

$$C_{\text{ext}} = C_{\text{scat}} + C_{\text{abs}} = k^4 |\alpha|^2 / 4\pi + k\alpha'' \quad (3)$$

where k is the wave number, $k = 2\pi n/\lambda$ and α'' denotes the imaginary part of the polarizability. The direction of the resulting radiation pressure points along the axis of the beam and hence acts to destabilize the trap in the axial direction. However, by tightly focusing the light in the axial direction, \mathbf{F} can overcome

\mathbf{F}_{rad} and stable trapping of nanoparticles can be achieved in three dimensions [6]–[8], [21], [23], [35].

A critical factor for optical trapping is the particle material which has great influence on the trapping stability through the polarizability α [see equations (1) and (2)]. \mathbf{F} and \mathbf{F}_{rad} scale linearly and quadratically, respectively, with the polarizability which in turn scales with the polarizable volume, V , of the nanoparticle:

$$\alpha = 3V \frac{\varepsilon_p - \varepsilon_m}{\varepsilon_p + 2\varepsilon_m}. \quad (4)$$

Here, ε_m refers to the dielectric permittivity of the medium and ε_p to that of the particle at the appropriate wavelength [36]. The simple relation in equation (4) is only valid for very small nanoparticles that behave as true dipoles ($d \ll \lambda$). If the particles are coated, the coating will also affect the total polarizability of the particle. The effect of a coating layer was quantified in [37] where they extended equation (4) in order to include a coating layer having a different dielectric constant than the core.

The quadratic scaling of \mathbf{F}_{rad} with α means that the trap becomes destabilized for larger reflective (metallic) particles. The absorption cross section scales with particle volume and absorption leads to heating. This causes dramatic heating of irradiated

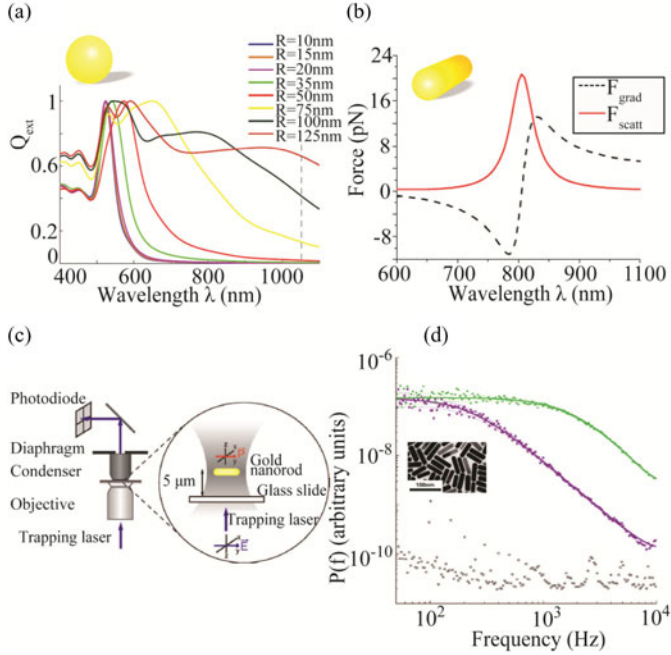


Fig. 2. Resonant versus non-resonant trapping of gold nano-spheres and -rods. (a) Extinction cross section of gold nano-spheres with radii ranging from 10 nm to 125 nm calculated using Mie’s equations, the vertical dashed line denotes 1064 nm, the wavelength with which the experiments depicted in Fig. 1 were carried out. (b) Calculated optical forces on a nanorod (15 nm \times 60 nm) for wavelengths near the plasmon resonance, reproduced with permission from [45]. (c) Optically trapped single gold nanorods which align with the laser polarization, reproduced with permission from [40]. (d) Power spectra of time series from two trapped nanorods, green: 85.1 ± 7.3 nm \times 44.1 ± 6.5 nm, purple: 41.2 ± 8.3 nm \times 8.3 ± 1 nm. Lorentzian fits are shown as full lines and black circles represent data from an empty trap. Reproduced with permission from [40].

metallic particles with non-vanishing imaginary polarizability, α'' , more details on this are given in Section V.

B. Resonant Versus Non-Resonant Trapping

The particle polarizability, α , in equations (3) and (4) is wavelength dependent and can exhibit a resonance in the optical or NIR spectrum. Therefore, the gradient force, the radiation force, and the particle absorption change dramatically across such a resonance. The gradient force can even become repulsive due to a negative polarizability when the laser wavelength is shorter than the resonant wavelength [10], [20]. Nanoparticles often have a distinct peak in the polarizability spectrum (as shown in Fig. 2(a) where C_{ext} from equation (3) is plotted as function of λ). In the following, trapping at resonance will refer to trapping using a wavelength overlapping with the peak polarizability, whereas off-resonant trapping refers to trapping using a wavelength which is several hundred nanometers away from the peak. For a more elaborate description of the effect of resonance on trapping please see [38].

Plasmonic resonances in metallic particles are due to resonant field induced oscillations of the conduction electrons. At resonance, absorption and scattering are strongly enhanced [39]. Metallic gold nanoparticles have resonances in the middle of the visible spectrum, as plotted in Fig. 2(a). These resonances red

shift and broaden with increasing particle size. Gold nanorods can be designed to be resonant with nearly any visible or NIR wavelength by appropriately choosing the aspect ratio [15]. As shown in Fig. 2(b) the forces on a nanorod depend strongly on the proximity of the trapping wavelength to the resonance, in this case the resonance is located just above 800 nm. Gold nanorods can be individually optically trapped by NIR lasers and align with the polarization of the laser [40]–[42], as sketched in Fig 2(c). Tunable resonances are also obtained with composite nanoparticles like gold nanoshells by appropriately choosing the thickness of the gold layer decorating the silica core [19], [43].

III. QUANTIFICATION OF INTERACTIONS BETWEEN PARTICLE AND OPTICAL TRAP

A. Dynamics of a Trapped Nanoparticle

An optical trap based on a laser with a Gaussian intensity profile exerts a harmonic force on the trapped object. Hence, the trapping potential has the following form:

$$U = \frac{1}{2} \kappa_x (x - x_0)^2 \quad (5)$$

where κ_x is the spring constant characterizing the trapping potential along the x -direction (coordinate system as in Fig. 1) and x_0 is the equilibrium position. The corresponding harmonic force on the particle is simply $F_{\text{trap}} = -\kappa_x (x - x_0)$. Optically trapped nanoparticles typically undergo significant thermal diffusion within the trapping volume. The characteristic escape time from the trapping potential, τ_{esc} , is given by $\tau_{\text{esc}} = \tau_0 \exp(U/k_B T)$ [44], where $k_B T$ is the thermal energy and $1/\tau_0$ is the attempt frequency. Therefore, a potential depth of a few times the thermal energy is sufficient for stable trapping of a nanoparticle. Expressions similar to equation (5) apply also in the two other translational directions, however, with different spring constants, κ_y and κ_z . Typically, κ_z is significantly weaker than κ_x and κ_y because it is more difficult to tightly focus the light in the axial direction, resulting in a less steep axial intensity gradient.

The resulting force acting on a nanoparticle in an optical trap is not easily calculated. Therefore, it is common procedure to calibrate the trapping potential in order to quantify the spring constants κ_x , κ_y , and κ_z which then characterize the 3-D trapping potential and can be used for force determination. For a nanoscopic particle which cannot easily be visualized while trapped, calibration is most conveniently and precisely done by passively measuring the Brownian fluctuations of the particle in the trap, see Section III-B.

The distribution of positions visited by a particle exploring a potential U in one dimension, x , is given by Boltzmann’s distribution:

$$P(x) = P_0 e^{\left(-\frac{U(x)}{k_B T}\right)} \quad (6)$$

where P_0 is a normalization constant (the inverse partition function). For a harmonic potential, the standard deviation, σ_x , of this distribution is given by the Equipartition Theorem:

$$\sigma_x = \sqrt{\frac{k_B T}{\kappa_x}}. \quad (7)$$

A measurement of the standard deviation of the particle positions therefore provides κ_x . The expressions in (6) and (7) apply to all translational directions with distinct κ_x , κ_y , and κ_z .

A more popular and robust method (less prone to drift) to determine κ_x , κ_y , and κ_z is to consider the power spectral density of the particle's fluctuations in the trap [46]. The motion of the particle is well described by the Langevin equation, the power spectrum of which yields a Lorentzian function:

$$P(f) = \frac{k_B T}{\gamma} \frac{1}{f^2 + f_c^2}. \quad (8)$$

Here, $f_c = \kappa/2\pi\gamma$ is denoted the corner frequency and is the ratio of the spring constant κ (κ_x , κ_y , or κ_z) and the Stokes drag $\gamma = 6\pi\eta r$. η is the viscosity of the media and r the radius of the particle. Examples of powerspectra recorded with gold nanospheres are shown in Fig. 1(b) [6] and with gold nanorods in Fig. 2(d). From the powerspectrum f_c and consequently κ can be determined, thus fully characterizing the interaction between the nanoparticle and the optical trap. Examples of how κ varies with particle size and material are shown in Figs. 1(c), 1(d), 4(c), and 5(b).

B. Particle Position Detection

As a nano-scopic particle is relatively difficult to visualize and since this visualization becomes even more challenging because of its rapid thermal fluctuations within the trapping volume, the nanoparticle's positions are most conveniently and precisely measured by means of a photodiode. A quadrant photodiode (QPD) can detect the interferometric pattern of the forward scattered laser light, and from this the particle's position can be determined. This approach offers great time resolution (microsecond) as well as nanometer spatial accuracy [47]. Determination of the lateral positions relies on a linear relation between the particle position in the trap and the difference in light intensity incident on four quadrants. The axial position scales linearly with the total intensity incident on all four quadrants, thus allowing for 3-D calibration [47]. Photodiodes are typically fabricated to have optimal performance in the visible spectrum and severe filtering of high frequencies typically takes place while using NIR light [48]. This effect, as well as aliasing, needs to be taken into account in order to perform an accurate calibration [49].

While there exist other ways to detect nanoparticles than QPD detection (see Section VII) it is essential, for accurate calibration, that the particle positions are captured within a short time interval (<1 ms) to minimize position averaging effects. This is particularly important for nanoparticles that diffuse faster than microscopic particles.

IV. OPTICAL TRAPPING OF NANOPARTICLES

A. Dielectric Particles

Conventional materials used in optical trapping include silica and polystyrene. These materials have indexes of refraction higher than that of water at NIR wavelengths which is a necessary condition for achieving stable optical trapping in water.

Experimental and theoretical quantification of the trapping potentials of polystyrene particles was rigorously performed by Rohrbach [21], see Fig. 1(d). The spring constants increase approximately linearly with particle size for all translational directions up to a particle size of approximately $1 \mu\text{m}$ at which the particle size starts to exceed the size of the focal spot. At this point the assumption behind equation (1) (that $\lambda \gg r$) clearly breaks down and F has to be cast as an integral over the particle volume. Using this approach, very good agreement was found between experimental and calculated values of κ for polystyrene particles [21]. Theoretical calculations of trapping forces have also been carried out for other dielectric constants and particle sizes both in presence and absence of spherical aberration [22], [23], [47], which is treated in more detail in Section VI.

B. Metallic Nanoparticles

Gold nanoparticles have significantly higher polarizability, even when trapped off-resonance, and offer improved trapping stability compared to polystyrene nanoparticles. A direct comparison between polystyrene and gold trapping was performed by Svoboda *et al.* [7] where the maximum force applied to $D = 36.2 \text{ nm}$ gold nanoparticles was found to be ~ 7 times higher than the maximum force that could be applied to equivalent polystyrene particles. This ratio was found to correlate well with the ratio between the polarizability of the gold and polystyrene nanoparticles thus confirming the importance of a high polarizability in efficient trapping.

Optical trapping of gold and other metallic nanoparticles has now been reported by several groups and focus has been on both quantification of trapping potentials and on characterizing the scaling of the trapping strength with particle size [6], [8], [10], [50]. One obstacle for achieving stable optical trapping of nanoparticles is the spherical aberration inherently present in essentially all focused laser spots, even when using a water immersion objective [51]. Different techniques have been developed to minimize spherical aberration, for instance by correcting the wavefront using an spatial light modulator (SLM) [52] or simply by using special immersion oils for the objective that minimize spherical aberration [9]. This increases the efficiency of the optical trap [see Fig. 7(c)] and is particularly useful for trapping deeper inside the imaging chamber [9]. Employing this technique, gold nanoparticles as small as 9 nm in diameter could be trapped [the results are shown in Fig. 1(c)] [8].

Metallic nanorods are now being intensively explored in optics due to their tunable resonance across the entire optical and NIR spectrum, see Fig. 2(b–d) [20], [40], and their extreme and orientation dependent heating properties [53]. The resonance peak sensitively red shifts with increasing aspect ratio and can be tuned into the NIR region for an aspect ratio of approximately 5. The transparency of biological materials in the NIR spectral window [54] makes such rods extremely interesting candidates in the context of photothermal applications [15].

Interestingly, a trapped nanorod aligns with the polarization of the trapping laser beam, see Fig. 2(c) [40], thus allowing for rotation of the particle by rotation of the laser polarization

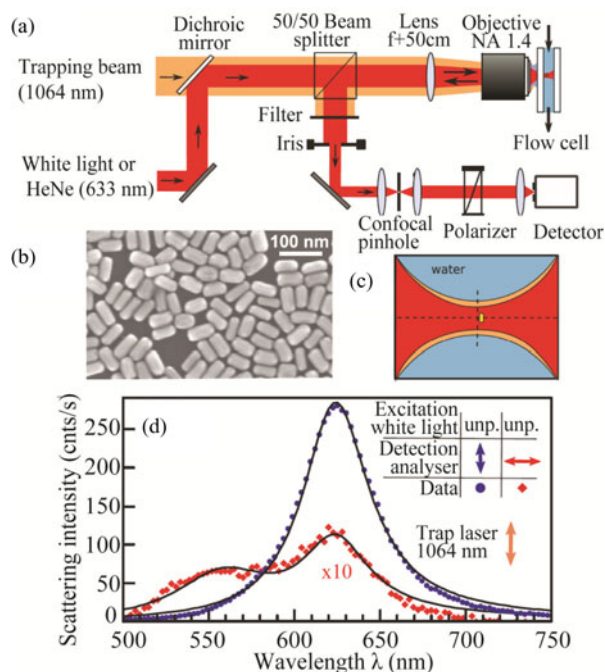


Fig. 3. Trapping and measuring the scattering from individual gold nanorods, reproduced with permission from [12]. (a)–(c) Nanorods, having dimensions $60 \text{ nm} \times 25 \text{ nm}$, align along the transverse laser polarization. (d) Collection of scattered white light polarized parallel or perpendicular to the polarization of the trapping laser. The scattered light with polarization parallel to the trapping polarization (blue circles) shows a peak corresponding to the longitudinal resonance of the rod at $\sim 630 \text{ nm}$. Scattered light with orthogonal polarization shows a peak corresponding to the transversal resonance at $\sim 550 \text{ nm}$ (red diamonds).

and for applying an optical torque on the particle [12]. Torques of magnitude around $100 \text{ pN}\cdot\text{nm}$ have been applied to gold nanorods by an optical trap (setup and results are shown in Fig. 3) [12], this being on the relevant scale for probing the torque of single molecule rotary motors. Related to trapping of nanorods is the optical manipulation of metallic nanowires in 3-D, where optical control of nanowires with lengths between 1 and $100 \mu\text{m}$ and aspect ratios up to 100 was accomplished [55]. By employing a different beam profile, a Fourier transformed Bessel beam generated with a spatial light modulator, nanowires could be aligned in the image plane along the laser polarization [56].

C. Quantum Dots

Semiconductor nanoparticles, also called quantum dots (QDs), are widely used in biology as photostable substitutes for fluorophores to label single proteins and cellular organelles [57]. The desire to optically control such QDs is motivated by the possibility of simultaneously imaging and performing force spectroscopy of QD conjugated molecules [58]–[60]. The wavelength of the fluorescent light emitted by a QD is inversely proportional to the size of the QD and hence a range of QD sizes exists that emit in the visible spectrum. Off-resonant trapping, using continuous wave NIR light, of a range of conventionally available individual CdSe QDs was reported by Jauffred *et al.* [59], [60]. The resulting spring constants characterizing the interaction between the EM field and the QD were found

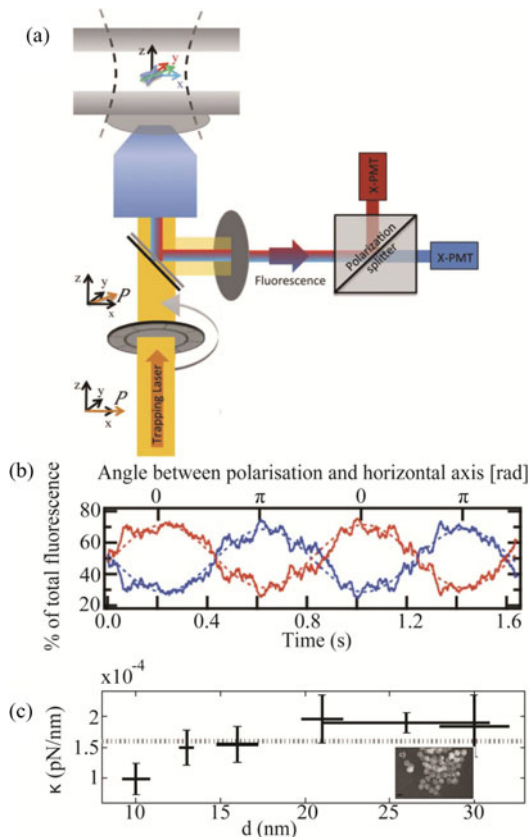


Fig. 4. Optical control of individual quantum dots. (a) Experimental setup to align and spin individual quantum rods in an optical trap. A polarization splitter is used to separate the x and y polarizations of the emitted light from the rod that is aligned with the laser polarization, reproduced with permission from [58]. (b) Polarization spectroscopy of a rod that rotates at a frequency of 50 Hz . Red and blue lines denote x and y polarization, respectively, dashed lines are sinusoidal fits to the data, reproduced with permission from [58]. (c) Quantification of the spring constants characterizing the optical trapping of individual QDs of various sizes, reproduced with permission from [59]. In all experiments trapping is done using a continuous wave (CW) NIR laser.

to be independent of the emission wavelength of the QD, see Fig. 4(c), and of comparable size to the spring constants characterizing metallic nanoparticle trapping.

Interestingly, the relatively weak CW trapping laser light can act as a source for two-photon excitation of the trapped QDs, thus eliminating the demand for an excitation light source for imaging of trapped QDs. This nonlinear effect is, however, only a weak perturbation to the overall trapping which is supported by the finding that the trapping stiffness scales linearly with laser power [59].

Quantum rods have elongated shapes and the polarization of the emitted light from a quantum rod depends on its orientation [experiment shown in Figs. 4(a)]. In Ref. [58] rotation of quantum rods with frequencies up to 320 Hz was achieved. Simultaneously, the rods were two-photon excited by the trapping laser beam and the linearly polarized emitted light measured. By splitting the emitted light in the vertical and horizontal components they found a clear sinusoidal relation between the polarization of the emitted light as a function of the orientation of the rod in the trap, see Fig. 4(b) [58]. These results pave the

way for a QD based system where trapping and visualization is further combined with the ability to measure and transduce torque at nano-scale. Possible further improvements through resonant trapping are theoretically described in [38].

Although a range of different materials are used for commercially available QDs, the material of choice in all reported QD trapping experiments has so far been CdSe whose optical properties were treated in [61]. It is possible that QD trapping efficiency could be improved by choosing QDs made from other semiconductor materials.

D. Hybrid Nanoparticles

Nanoparticles composed of a metallic shell and an inner dielectric core have shifted plasmonic resonances compared to spherical metallic nanoparticles of equal size [19]. The plasmon resonances of gold nanoshells encapsulating a silica core, can be readily tuned across the optical spectrum by changing the ratio between the shell thickness and the diameter of the silica core [19]. NIR resonant gold nanoshells can be designed to produce severe heating upon irradiation with NIR light in the same manner as gold nanorods. Gold nanoshells might be more promising as photothermal absorbers in therapeutic applications, compared to, e.g., gold nanorods, due to their lower cytotoxicity [46].

The possible influence of the resonance in optical trapping of gold nanoshells was recently explored by tuning the wavelength of the laser across a spectral range (from 720 to 850 nm) near the plasmon resonance of the gold nanoshells [62]. The spring constants characterizing the trapping potential were found to be nearly independent of the proximity of the trapping wavelength to the plasmon resonance of the nanoshell. However, the quantification of the exact trapping strength was complicated by heating effects which also depended on the wavelength and consequently changed the effective viscosity [62].

We quantified the trapping potential of gold nanoshells trapped off-resonance at a wavelength of $\lambda = 1064$ nm. The gold nanoshells employed had a broad resonance peak at ~ 875 nm (see Fig. 5(b), upper left inset) making these nanoshells interesting candidates for biomedical applications due to the transparency of biological material in the NIR region [54]. By using the photodiode detection scheme sketched in Fig. 1 and explained in detail in [48] and the MATLAB procedures from [49] we quantified the trapping potential of gold nanoshells having a silica core of 118 nm and a gold layer of ~ 15 nm [drawn in the lower right inset in Fig. 5(b)], coated with PEG 5 kD.

The harmonic shape of the position histogram, shown in the inset of Fig. 5(a), as well as the Lorentzian shape of the power spectrum [see Fig. 5(a)], shows that the gold nanoshells were trapped in a harmonic potential.

Fig. 5(b) shows the lateral spring constant as a function of laser power. As shown by the full line there is a linear relation between the spring constant and the laser power, which is a hallmark of optical tweezing and an indication that no significant heating occurs. This observation is consistent with the reportings of Jain *et al.* [63] who showed that nanoshells with dimensions similar to those used in the current study dominantly scatter light whereas only little absorption occurs.

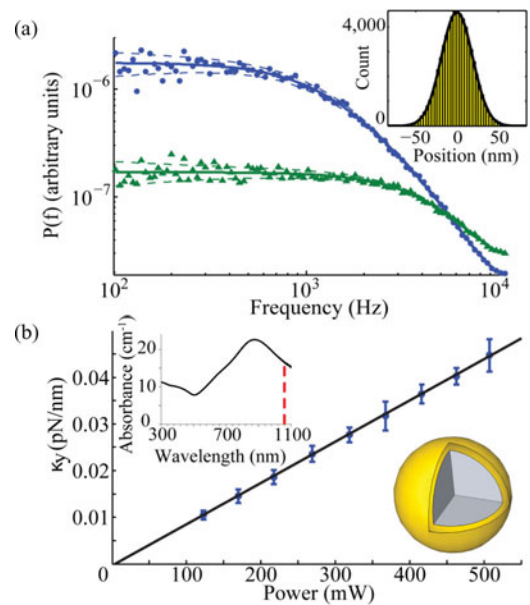


Fig. 5. Quantification of NIR trapping of gold nanoshells. (a) Power spectra of the time series for a trapped gold nanoshell with a $d = 118$ nm silica core and a 15 nm thick gold shell. The laser power at the sample was $P = 508$ mW (green triangles) or $P = 123$ mW (blue circles). Inset shows the position distribution of a gold nanoshell trapped at $P = 123$ mW, full lines denote Lorentzian fits [49]. Inset shows Gaussian position histogram. (b) Spring constant versus laser power measured for gold nanoshells ($n = 12$), the full line denotes a linear fit to data. Upper left inset shows the optical absorbance of the gold nanoshells, dashed red line denotes the 1064 nm trapping laser wavelength. Lower right inset is a drawing of the gold nanoshell.

Interestingly, an extrapolation of the curve down to 50 mW, the laser power used in [62], yields a value for the spring constant which is quite close to the nearly constant value measured in [62] (~ 5 pN/ μm). This is despite the facts that the shells employed had a different resonance peak and that the trapping lasers had different wavelengths. This supports the finding that the trapping strength is not sensitively dependent on the particle resonance wavelength with respect to the trapping wavelength.

E. Comparing Various Nanoparticles

The optical properties of the nanoparticles reviewed in the preceding sections are summarized in Table I. This table provides the currently available information on the theoretically calculated and experimentally measured polarizabilities, on the measured spring constants, and on the maximum forces exerted. The theoretical values of the polarizability, α_{calc} , were found by using equation (4) or, for particles as CdSeZnS and gold nanoshells with a coating/shell, the modified version from [37]. For the composite QD we employed a $d = 5.3$ nm core having $\varepsilon = 6.55$ [64] and a biological coating having $\varepsilon = 2.10$, whereas in [59] the whole QD structure was assumed to be made of CdSe. Experimental values for all α_{exp} were obtained from the reported κ_{exp} by using the procedure given in [60].

The discrepancies found between α_{calc} , and α_{exp} could be due to several factors. One is that equation (4) is not very accurate for particles larger than ~ 10 nm. Another source of error is that the red-shifted resonances of the larger metallic nanoparticles are not accounted for by equation (4), this

TABLE I
OPTICAL PROPERTIES FOR VARIOUS NANOSTRUCTURES

Type	α_{calc} [\AA^3]	α_{exp} [\AA^3]	κ_{exp} [pN/nm/W]	F_{MAX}/P	REF
PS 38nm	2.55×10^6	-	-	0.09 pN/W	[7]
AuNP 36nm	8.2×10^7	4.1×10^{10}	5.0×10^{-3}	0.6 pN/W	[7]
AuNP 194nm	1.3×10^{10}	2.2×10^{12}	0.3	38.0 pN/W	[8]
AuNP 254nm	2.8×10^{10}	4.1×10^{12}	0.5	68.0 pN/W	[8]
AgNP 40nm	1.1×10^8	7.4×10^{10}	9.0×10^{-3}	-	[50]
QD, CdSe 5/26nm	1.9×10^6	2.4×10^7	1.6×10^{-3}	-	[59, 60]
SiAuNS 118/15nm	6.3×10^9	-	8.0×10^{-2}	-	This work
SUV 50nm	1.2×10^7	8.2×10^9	1.0×10^{-3}	-	[25]
AuNR (60x25nm)	^a	^a	1.5×10^{-2}	100 pNnm [¶]	[12, 40]

All values in the table are obtained using a trapping wavelength $\lambda = 1064$ nm.

^a Experimental and calculated polarizabilities for rods can be found in Ref. [40] for a range of aspect ratios and particle volumes. [¶] The maximum torque that could be applied on a rod [12].

could increase the polarizability. Finally, the experimental values, α_{exp} , were found by the procedure outlined in [60] which assumes that the intensity distribution is perfectly Gaussian and that the particle is located at the peak of the intensity. In practice, a trapped metallic nanoparticle is most likely displaced from the center [35] and the focal intensity distribution is not perfectly Gaussian [65], these effects lead to an overestimate of α_{exp} .

V. OPTICALLY INDUCED HEATING

In a typical optical trapping experiment the intensities reach MW/cm^2 at the focus. Potential heating caused by this intense light flux can have detrimental effects on proteins or living cells that might be near or within the laser focus. Of particular concern is the trapping of absorbing nanoparticles like metal particles having plasmon resonances near the trapping wavelength. Such particles can easily reach temperatures near the critical temperature of water and even at much lower temperature elevations radically alter the physical environment, e.g., the viscosity of water. Therefore, it is essential to quantify and take into account the laser induced heating in any application where potential absorption of light takes place.

Several assays have been designed to assess the temperature generated by laser irradiation of nanoparticles fixed to a substrate [53], [66], [67]. However, only few assays have been employed to quantify the heating of nanoparticles that are trapped in 3-D [2], [12]–[14]. One inherent problem complicating trustworthy temperature calculations is that the focal intensity distribution at the nanometer level is unknown and the exact position of the nanoparticle with respect to the focal intensity distribution is difficult to access. For this reason, direct measurements that do not involve a priori assumptions about the position of the particle and focal intensity distributions, are highly desirable.

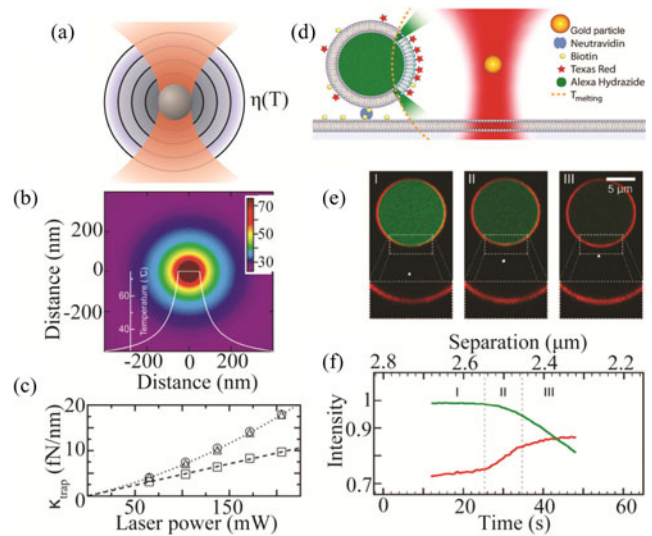


Fig. 6. Different assays to quantify heating of optically trapped nanostructures. (a) Heat radiating from a trapped nanoparticle lowers the viscosity of the nearby solution thus affecting the Brownian motion of the particle. (b) and (c) Heating from an optically trapped gold nanoparticle, $d = 100$ nm, figure reproduced with permission from [14]. A Mie calculation of the temperature profile is plotted in (b), the trapping spring constants found by power spectral analysis (triangles), Stokes drag (circles), and the Equipartition Theorem (rectangles) are plotted in (c). (d)–(f) A gel phase GUV, with melting temperature $T_m = 33$ °C, contained a dye in the lumen. The GUV was approached by a trapped gold nanoparticle. By measuring the distance, D , for the onset of GUV leakage the particle temperature was inferred from the simple relation, $T \propto 1/D$, figure reproduced from [13] with permission. Images from the experiment are shown in (e) and time evolution of the membrane and lumen fluorophores in (f).

One of the first quantifications of the heating of optically trapped silica and polystyrene particles ($d \sim 500$ nm) was performed by measuring the changes in the Brownian fluctuations caused by a temperature dependent change of the viscosity of water, as depicted in Fig. 6(a) [68]. The resulting temperature increase during trapping of micron sized polystyrene particles in glycerol and water were found to be on the order of 10 K and 1 K, respectively, at typical trapping laser powers. The temperature increase was attributed to the absorption of NIR light primarily by the solution and not by the dielectric particle [68]. Recent experiments using quantum dot luminescence thermometry have confirmed that heating of an intracellular aqueous environment exposed to NIR wavelengths is indeed on the order of 1 K at typical trapping laser powers [69].

A similar strategy was adopted to quantify the temperature increase of a trapped 100 nm gold nanoparticle [14]. The particle temperature was found through a combination of measurements of the nanoparticle's Brownian motion and Mie calculations, as shown in Fig. 6(b) assuming knowledge of the particle's location within the intensity profile. They found temperature elevations up to ~ 90 °C at $P = 200$ mW at the surface of the nanoparticle. A linear relation between the spring constant characterizing the optical trapping and the power used is a hallmark of optical trapping. As shown by the triangles in Fig. 6(c), a non-linear relation was found, this being attributed to decreased viscosity of the surrounding liquid caused by the temperature elevation at the surface of the irradiated particle. Correcting the viscosity with a temperature dependent factor returned the expected linear

relation [squares in Fig. 6(c)]. The heating rate for a 100 nm gold nanoparticle was found to be 266 K/W [14].

Other assays designed to measure the heating of irradiated nanoparticles have used a surrounding matrix that can undergo a phase transition at a given temperature as a heat sensor. Such heat sensors have utilized the ice to water phase transition [70] or lipid bilayers undergoing gel to fluid phase transitions [13], [66], [71]. Lipid bilayer phase melting can be visualized by several methods: 1) onset of lipid mobility [71], 2) phase dependent partitioning of certain lipophilic tracer dyes [53], [66], [72], or 3) permeabilization of the lipid bilayer to aqueous fluorophores [13].

The heating of different sizes of gold nanoparticles trapped in three dimensions was recently quantified in an assay schematically shown in Fig. 6(d). A Giant Unilamellar lipid Vesicle (GUV) with a phase transition at $T_m = 33^\circ\text{C}$, was immobilized on a supported lipid bilayer by streptavidin-biotin conjugation. Subsequently, a gold nanoparticle was trapped and brought closer to the GUV at constant velocity. At a certain distance, D_m , the heat radiating from the trapped gold nanoparticle caused the GUV temperature to reach T_m and the GUV became leaky, this being visible by efflux of the encapsulated fluorescent molecules, and an up-concentration of bilayer fluorophores into the fluid membrane phase, see Fig. 6(e) and (f). Since the temperature profile decays as $T(D) \sim 1/D$ away from the nanoscopic particle, knowledge of D_m and T_m renders it possible to deduce the entire temperature profile. One advantage of this method is that it contains no a priori assumptions regarding the focal intensity distribution or the location of the particle.

Surprisingly, the heating of gold nanoparticles trapped in three dimensions did not simply increase monotonically with particle size [13]. For particle diameters exceeding 100 nm the heating was found to decrease implying that the larger particles were stably trapped away from the center of the focus [see Fig. 7(b)] and hence not be exposed to the maximum focal intensity.

Heating is proportional to absorption; hence, it is not so surprising that the heating of irradiated gold nanorods was found to be dependent on rod orientation with respect to laser polarization [53]. Also, compared to their volume, gold nanorods were found to be extremely effective light to heat converters (in the right orientation). In fact, even at 20 mW the heat was sufficient to melt and reshape the rod into a more spherical shape.

While dielectric nanoparticles can be safely trapped at high powers with minimal heating, the heating of irradiated metallic particles is size, shape, and orientation dependent and can easily reach temperatures approaching the critical temperature of water ($T_c = 647\text{ K}$) at which the water phase is not stable any longer and explosive heating will occur [73].

VI. SPHERICAL ABERRATION

To achieve 3-D trapping it is common to use either high NA oil immersion or water immersion objectives to achieve a tight focusing of the laser beam. Focusing of light to a diffraction limited spot of size $\lambda/2$ results in spherical aberration [74].

Additionally, the light must pass water/glass interfaces to enter the aqueous chamber containing the objects to be trapped. Refraction at a water/glass interface significantly changes the

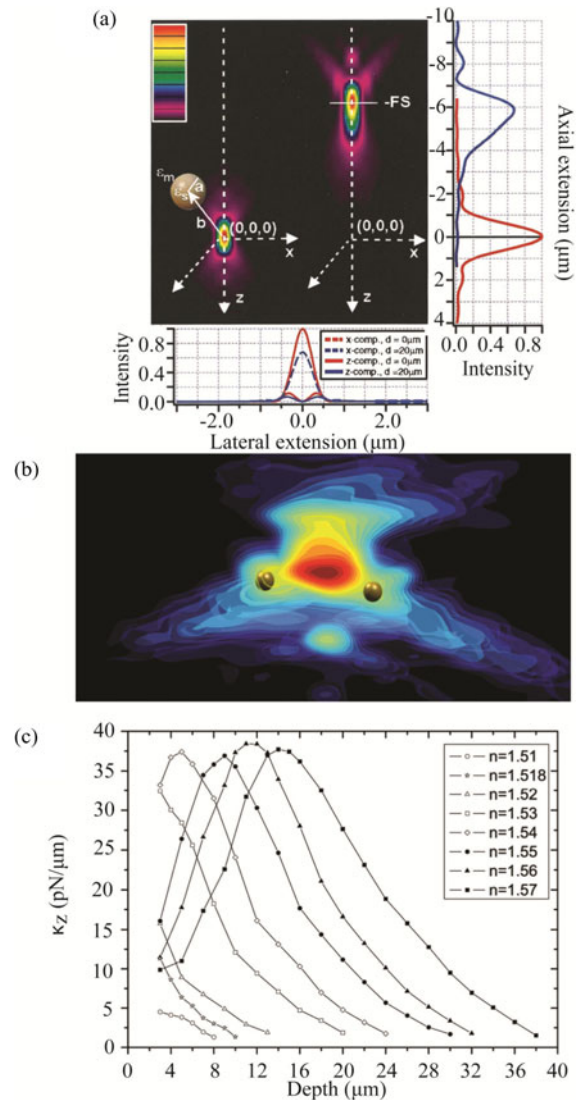


Fig. 7. Effect of spherical aberration in an optical trap. (a) Simulated focal intensity distributions obtained after focusing NIR light ($\lambda = 1064\text{ nm}$) by an oil immersion objective through a glass-water interface, reproduced with permission from [74]. (b) Experimentally measured focal intensity distributions within an optical trap focused by a water immersion objective, reproduced with permission from [35], 200 nm gold nanoparticles stably trapped before the focus. (c) Axial spring constants versus distance to the glass-water interface measured for a range of oils having different index of refraction, reproduced with permission from [9].

shape of the focus intensity distribution of light focused by an oil immersion objective, see Fig. 7(a) [74]. The refraction of light at the water/glass interface causes peripheral rays to converge at different depths inside the chamber relative to rays lying closer to the beam axis, thus resulting in an axially elongated focal volume. Especially for oil immersion objectives, the aberration of the optical trap increases with distance away from the glass surface and often leads to loss of trapping ability at axial depths of tens of micrometers.

Since the origin of spherical aberration originates from the refractive index mismatch at the water/glass interface it is possible to compensate these effects by changing the index of refraction of the immersion oil between the glass and the objective. In reference [9] a series of immersion oils with different refractive

indexes was used to trap particles at different heights from the cover glass surface, the measured axial spring constants as function of trapping depth and immersion oil refractive index are shown in Fig. 7(c). An important conclusion is that the axial trapping constant at a depth of 5–10 μm , can be increased almost by a factor of 7 by using an oil with $n_{\text{oil}} = 1.54$ instead of the conventional oil used in microscopy ($n_{\text{oil}} = 1.518$).

Water immersion objectives are typically optimized for visible light and cause spherical aberration of a trapping NIR laser beam. The aberration can, however, be minimized by adjusting the correction collar of the objective [75], and one advantage of the water immersion objective is that the spherical aberration does not change with trapping depth.

Recently, Kyrsting *et al.* mapped the 3-D focal distribution of an optical trap ($\lambda = 1064$ nm) focused by a water immersion objective or oil immersion objective using different immersion oils [13]. As expected, the intensity distributions were strongly sensitive to the immersion medium used and local intensity maxima were observed off-axis and in front of the focal spot as shown in Fig. 7(b). Interestingly, this study also revealed that 200 nm gold nanoparticles stably trap at a position before the intensity maximum [as depicted in Fig. 7(b)] [13]. This is consistent with the heat profile observations [13] implying that larger trapped metallic nanoparticles needed to be displaced from the maximum intensity.

VII. VISUALIZATION OF NANOPARTICLES

Köhler illuminated bright field microscopy is often used in conjunction with optical trapping to visualize particles. However, the low contrast d makes it difficult to detect even metallic particles. Another modification of transmitted light microscopy yielding better contrast, is Differential Interference Contrast microscopy (DIC) which has been employed to visualize gold nanoparticles of tens of nanometer size [6], [7]. This method depends on the insertion of polarizers and Wollaston prisms in the imaging light path to convert phase contrasts to intensity contrasts in the resulting image.

Confocal microscopy operated in reflection mode can also be used to visualize trapped nanoparticles. This method strongly depends on the reflectance, i.e., the ratio of illumination intensity to reflected intensity. Confocal reflection visualization of very small nanoparticles in the optical trap has been demonstrated [35], [50] and the plasmonic resonances of the particles make them scatter some wavelengths more efficiently than others.

Other methods for visualizing nanoparticles in an NIR optical trap often rely on detection of nanoparticle fluorescence or on elastic scattering of incident light. If the trapped nanostructure incorporates fluorophores, they might become excited by simultaneously absorbing two photons from the trapping NIR beam [59], [76]. This effect is shown for a 200 nm polystyrene nanoparticle (PS) in Fig. 8(a) left. An advantage of the two-photon visualization is that it allows the nanoparticle to be visualized only with a sensitive camera and without the need of additional light sources. Imaging by two-photon excitation by the trapping laser can be implemented in any epifluorescence microscope equipped with a sensitive CCD camera or a photo-

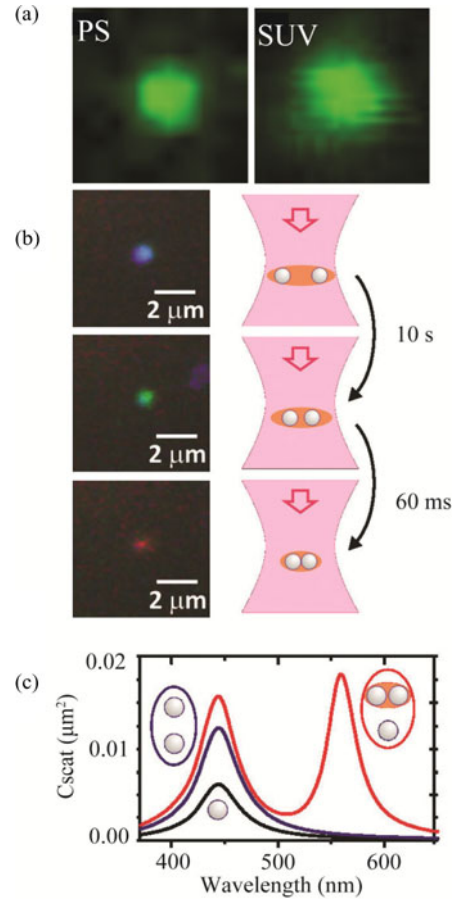


Fig. 8. Imaging of nanoparticles in an optical trap. (a) Left image shows a $d = 200$ nm polystyrene nanoparticle labeled with Alexa Fluoro Hydroxide, with absorption maximum at 502 nm, and excited by two-photon absorption of the trapping laser beam. Right image shows the emission from a DiOC_{18:2} labeled SUV ($d = 70$ nm) held by an optical trap and imaged using confocal scanning microscopy. (b) Color recorded by dark field microscopy of trapped silver nanoparticles, reproduced with permission from [2]. (c) Corresponding simulated scattering spectra for individual and aggregated silver nanoparticles, reproduced with permission from [2].

multiplier tube combined with hot mirrors and color filters to block the trapping laser light from reaching the detector. Also, trapped metallic nanoparticles can be two-photon excited by an additional pulsed and mode-locked laser focused to the same point in space as the trapping laser [5], [41]. One advantage of two-photon fluorescence is that the large frequency difference between the excitation beam and the emission makes it easy to distinguish signal from background illumination.

A combined confocal microscope and optical trap can also be used to visualize fluorescent trapped nanoparticles, as shown for a trapped Small Unilamellar lipid Vesicle (SUV) in Fig. 8(a) right [25].

Dark field microscopy is a very efficient visualization method for nanoparticles based on elastic scattering of incident light. The dark field method relies on detecting only the light scattered from the nanoparticle and not the illuminating beam. Combining dark field microscopy with optical trapping of nanoparticles is a challenge as it requires a balance between a high NA needed for stable optical trapping (typically $\text{NA} = 1.3$ – 1.4) and a NA

of the objective that is lower than the NA of the condenser for dark field imaging [77]. Methods for circumventing this strict requirement usually compromise either the trapping stiffness by using a low NA for the objective [78], [79] or the possibility of spectroscopic measurements by using a perpendicular laser for imaging [20], [80]. Recently a method was proposed in which both strong trapping and spectroscopic measurements can be achieved by collecting back-scattered light through an aperture that blocks reflected light from the specimen [81]. Another method demonstrated plasmonic coupling of metallic nanoparticles suspended in an optical trap using dark field microscopy by only constraining the NA in the imaging channel while maintaining a high NA of the trapping laser [see Fig. 8(b) and (c)] [2]. This study revealed a gradual red shift in the observed plasmon resonance because the particles gradually aggregated.

VIII. FUTURE DIRECTIONS

Nanoparticles can be trapped in relatively weak potentials in which they perform substantial Brownian fluctuations compared to trapped micrometer sized dielectric particles. Therefore, trapped nanoparticles have great potential as ultrasensitive sensors of potentials or for localizing matter at nanoscale. The sensitivity of trapped nanoparticles allows, e.g., for weak acoustic vibrations to be picked up by the trapped nanoparticle as recently demonstrated, see Fig. 9(a) and (b) [82]. This elegant experiment opens up a range of new possibilities to explore the acoustic environment and communication inside and between cells or to measure the dynamics of cellular organelles as, e.g., the rotating bacterial flagellum. Weakly trapped nanoparticles also hold great promise as ultrasensitive force transducers useful, e.g., for measuring thermophoretic effects [83] or for investigating the force properties of molecular motors.

Recently, it was shown that an optical trap could be employed to precisely pattern gold nanoparticles on a substrate [84], and an increased control over individual nanoparticles pave the way for realizing nano-architecture in 3D [see Fig. 9(c)]. We also anticipate that optical trapping will become a useful tool in the rapidly expanding field of plasmonics where multiple optical traps with controllable separation [28] will be very useful for studying collective biophotonical effects such as optical binding [3] without interfering substrates.

The efficiency of optical trapping relies on the size of the focus and hence is limited by the diffraction limit. Recent research is focusing on concentrating light to subdiffraction scales by using plasmonic structures to yield superior localization of the nanoparticles at much laser powers [32], [33]. However, the functionality of such plasmonic traps is compromised due to the necessity of having fixed plasmonic structures nearby and the potential heating effects. Future experiments would aim at quantifying the heat generated by the plasmonic devices and implementing these in biological applications.

In the future, optical trapping of nanoparticles will also contribute with exciting fundamental knowledge regarding light-matter interactions of nanostructures whose optical properties are largely unknown and certainly differ substantially from the corresponding bulk properties. These extraordinary properties giving promise of applications yet beyond imagination.

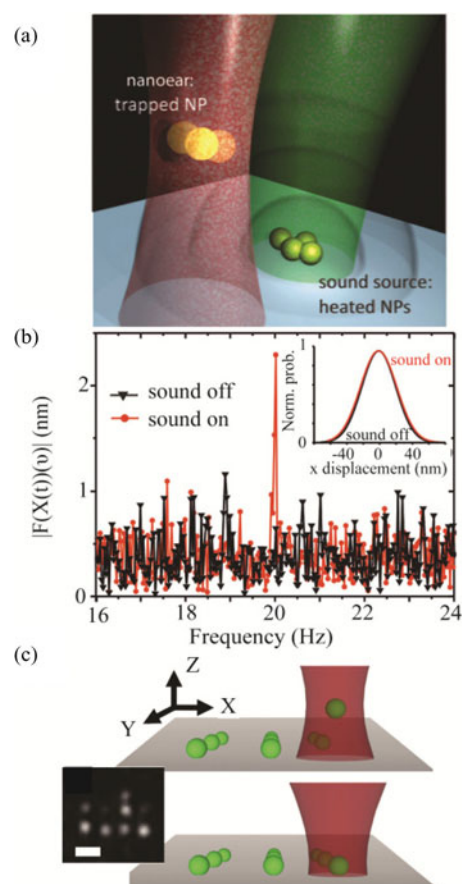


Fig. 9. Future applications of optical trapping of nanoparticles. (a)–(b) A gold nanoparticle, the so-called ‘nano-ear’, is optically trapped while an acoustic wave is generated nearby by heating of other nanoparticles. As visible in the power spectrum shown in (b), this weak acoustic wave is picked up by the trapped particle, reproduced with permission from [82]. (c) Optical trap mediated nanopatterning of gold nanoparticles on a glass substrate. The $d = 40$ nm gold nanoparticles were positioned on the surface with a precision of 100 nm and imaged using dark field microscopy, reproduced with permission from [84].

REFERENCES

- [1] L. Tong, H. Wei, S. Zhang, Z. Li, and H. Xu, “Optical properties of single coupled plasmonic nanoparticles,” *Phys. Chem. Chem. Phys.*, vol. 15, pp. 4100–4109, Mar. 28, 2013.
- [2] A. Ohlinger, S. Nedev, A. A. Lutich, and J. Feldmann, “Optothermal escape of plasmonically coupled silver nanoparticles from a three-dimensional optical trap,” *Nano Lett.*, vol. 11, pp. 1770–1774, Apr. 13, 2011.
- [3] K. Dholakia and P. Zemanek, “Colloquium: Gripped by light: Optical binding,” *Rev. Mod. Phys.*, vol. 82, pp. 1767–1791, 2010.
- [4] J. Chen, J. Ng, Z. Lin, and C. T. Chan, “Optical pulling force,” *Nat. Photon.*, vol. 5, pp. 531–534, 2011.
- [5] Y. Jiang, T. Narushima, and H. Okamoto, “Nonlinear optical effects in trapping nanoparticles with femtosecond pulses,” *Nat. Phys.*, vol. 6, pp. 1005–1009, 2010.
- [6] P. M. Hansen, V. K. Bhatia, N. Harrit, and L. Oddershede, “Expanding the optical trapping range of gold nanoparticles,” *Nano Lett.*, vol. 5, pp. 1937–1942, Oct. 2005.
- [7] K. Svoboda and S. M. Block, “Optical trapping of metallic Rayleigh particles,” *Opt. Lett.*, vol. 19, pp. 930–932, Jul. 1, 1994.
- [8] F. Hajizadeh and S. N. Reihani, “Optimized optical trapping of gold nanoparticles,” *Opt. Exp.*, vol. 18, pp. 551–559, Jan. 18, 2010.
- [9] S. N. Reihani and L. B. Oddershede, “Optimizing immersion media refractive index improves optical trapping by compensating spherical aberrations,” *Opt. Lett.*, vol. 32, pp. 1998–2000, Jul. 15, 2007.
- [10] M. Dienerowitz, M. Mazilu, P. J. Reece, T. F. Krauss, and K. Dholakia, “Optical vortex trap for resonant confinement of metal nanoparticles,” *Opt. Exp.*, vol. 16, pp. 4991–4999, Mar. 31, 2008.

- [11] M. Selmke, M. Braun, and F. Cichos, "Photothermal single-particle microscopy: Detection of a nanolens," *ACS Nano*, vol. 6, pp. 2741–2749, Mar. 27, 2012.
- [12] P. V. Ruijgrok, N. R. Verhart, P. Zijlstra, A. L. Tchebotareva, and M. Orrit, "Brownian fluctuations and heating of an optically aligned gold nanorod," *Phys. Rev. Lett.*, vol. 107, pp. 037401-1–037401-4, 2011.
- [13] A. Kyrsting, P. M. Bendix, D. G. Stamou, and L. B. Oddershede, "Heat profiling of three-dimensionally optically trapped gold nanoparticles using vesicle cargo release," *Nano Lett.*, vol. 11, pp. 888–892, Feb. 9, 2011.
- [14] Y. Seol, A. E. Carpenter, and T. T. Perkins, "Gold nanoparticles: Enhanced optical trapping and sensitivity coupled with significant heating," *Opt. Lett.*, vol. 31, pp. 2429–2431, Aug. 15, 2006.
- [15] X. Huang, I. H. El-Sayed, W. Qian, and M. A. El-Sayed, "Cancer cell imaging and photothermal therapy in the near-infrared region by using gold nanorods," *J. Amer. Chem. Soc.*, vol. 128, pp. 2115–2120, Feb. 15, 2006.
- [16] C. Loo, A. Lowery, N. Halas, J. West, and R. Drezek, "Immunotargeted nanoshells for integrated cancer imaging and therapy," *Nano Lett.*, vol. 5, pp. 709–711, Apr. 2005.
- [17] L. R. Hirsch, R. J. Stafford, J. A. Bankson, S. R. Sershen, B. Rivera, R. E. Price, J. D. Hazle, N. J. Halas, and J. L. West, "Nanoshell-mediated near-infrared thermal therapy of tumors under magnetic resonance guidance," *Proc. Natl. Acad. Sci. U S A*, vol. 100, pp. 13549–13554, Nov. 11, 2003.
- [18] L. Osinkina, S. Carretero-Palacios, J. Stehr, A. A. Lutich, F. Jackel, and J. Feldmann, "Tuning DNA binding kinetics in an optical trap by plasmonic nanoparticle heating," *Nano Lett.*, vol. 13, pp. 3140–3144, Jun. 24, 2013.
- [19] S. Kalese, S. W. Gosavi, J. Urban, and S. K. Kulkarni, "Nanoshell particles: Synthesis, properties and applications," *Curr. Sci.*, vol. 91, pp. 1038–1052, 2006.
- [20] K. C. Toussaint, M. Liu, M. Pelton, J. Pesic, M. J. Guffey, P. Guyot-Sionnest, and W. F. Scherer, "Plasmon resonance-based optical trapping of single and multiple Au nanoparticles," *Opt. Exp.*, vol. 15, pp. 12017–12029, Sep. 17, 2007.
- [21] A. Rohrbach, "Stiffness of optical traps: Quantitative agreement between experiment and electromagnetic theory," *Phys. Rev. Lett.*, vol. 95, pp. 168102-1–168102-4, Oct. 14, 2005.
- [22] A. Rohrbach and E. H. K. Stelzer, "Three-dimensional position detection of optically trapped dielectric particles," *J. Appl. Phys.*, vol. 91, pp. 5474–5488, 2002.
- [23] A. Rohrbach and E. H. K. Stelzer, "Optical trapping of dielectric particles in arbitrary fields," *J. Opt. Soc. Amer. A. Opt. Image. Sci. Vis.*, vol. 18, pp. 839–853, Apr. 2001.
- [24] A. Ashkin, J. M. Dziedzic, J. E. Bjorkholm, and S. Chu, "Observation of a single-beam gradient force optical trap for dielectric particles," *Opt. Lett.*, vol. 11, pp. 288–290, May 1, 1986.
- [25] P. M. Bendix and L. B. Oddershede, "Expanding the optical trapping range of lipid vesicles to the nanoscale," *Nano Lett.*, vol. 11, pp. 5431–5437, Dec. 14, 2011.
- [26] D. Min, K. Kim, C. Hyeon, Y. H. Cho, Y. K. Shin, and T. Y. Yoon, "Mechanical unzipping and rezipping of a single SNARE complex reveals hysteresis as a force-generating mechanism," *Nat. Commun.*, vol. 4, pp. 1705-1–1705-10, 2013.
- [27] Y. Gao, S. Zorman, G. Gundersen, Z. Xi, L. Ma, G. Sirinakis, J. E. Rothman, and Y. Zhang, "Single reconstituted neuronal SNARE complexes zipper in three distinct stages," *Science*, vol. 337, pp. 1340–1343, Sep. 14, 2012.
- [28] K. Visscher, S. P. Gross, and S. M. Block, "Construction of multiple-beam optical traps with nanometer-resolution position sensing," *IEEE J. Sel. Topics Quantum Electron.*, vol. 2, no. 4, pp. 1066–1076, Dec. 1996.
- [29] A. Jonas and P. Zemanek, "Light at work: The use of optical forces for particle manipulation, sorting, and analysis," *Electrophoresis*, vol. 29, pp. 4813–4851, Dec. 2008.
- [30] M. Dienerowitz, M. Mazilu, and K. Dholakia, "Optical manipulation of nanoparticles: A review," *J. Nanophoton.*, vol. 2, pp. 021875-1–021875-32, 2008.
- [31] Y. Pang and R. Gordon, "Optical trapping of 12 nm dielectric spheres using double-nanoholes in a gold film," *Nano Lett.*, vol. 11, pp. 3763–3767, Sep. 14, 2011.
- [32] M. L. Juan, M. Righini, and R. Quidant, "Plasmon nano-optical tweezers," *Nat. Photon.*, vol. 5, pp. 349–356, 2011.
- [33] P. J. Reece, "Finer optical tweezers," *Nat. Photon.*, vol. 2, pp. 333–334, 2008.
- [34] Y. Harada and T. Asakura, "Radiation forces on a dielectric sphere in the Rayleigh scattering regime," *Opt. Commun.*, vol. 124, pp. 529–541, 1996.
- [35] A. Kyrsting, P. M. Bendix, and L. B. Oddershede, "Mapping 3D focal intensity exposes the stable trapping positions of single nanoparticles," *Nano Lett.*, vol. 13, pp. 31–35, Jan. 9, 2013.
- [36] P. B. Johnson and R. W. Christy, "Optical constants of the noble metals," *Phys. Rev. E.*, vol. 6, pp. 4370–4379, 1972.
- [37] C. F. Bohren and D. R. Huffman, *Absorption and Scattering of Light by Small Particles*. Hoboken, NJ, USA: Wiley, 1998, p. 149.
- [38] T. Iida and H. Ishihara, "Theoretical study of the optical manipulation of semiconductor nanoparticles under an excitonic resonance condition," *Phys. Rev. Lett.*, vol. 90, pp. 057403-1–057403-4, Feb. 7, 2003.
- [39] J. Rodríguez-Fernández, J. Perez-Juste, F. J. Garcia de Abajo, and L. M. Liz-Marzan, "Seeded growth of submicron Au colloids with quadrupole plasmon resonance modes," *Langmuir*, vol. 22, pp. 7007–7010, Aug. 1, 2006.
- [40] C. Sellhuber-Unkel, I. Zins, O. Schubert, C. Sonnichsen, and L. B. Oddershede, "Quantitative optical trapping of single gold nanorods," *Nano Lett.*, vol. 8, pp. 2998–3003, Sep. 2008.
- [41] M. Pelton, M. Liu, H. Y. Kim, G. Smith, P. Guyot-Sionnest, and N. F. Scherer, "Optical trapping and alignment of single gold nanorods by using plasmon resonances," *Opt. Lett.*, vol. 31, pp. 2075–2077, Jul. 1, 2006.
- [42] J. Trojek, L. Chvatal, and P. Zemanek, "Optical alignment and confinement of an ellipsoidal nanorod in optical tweezers: A theoretical study," *J. Opt. Soc. Amer. A. Opt. Image. Sci. Vis.*, vol. 29, pp. 1224–1236, Jul. 1, 2012.
- [43] H. Liu, D. Chen, F. Tang, G. Du, L. Li, X. Meng, W. Liang, Y. Zhang, X. Teng, and Y. Li, "Photothermal therapy of Lewis lung carcinoma in mice using gold nanoshells on carboxylated polystyrene spheres," *Nanotechnology*, vol. 19, pp. 455101-1–455101-7, Nov. 12, 2008.
- [44] N. G. Kampen, *Stochastic Processes in Physics and Chemistry*. Amsterdam, The Netherlands: North-Holland, 1992.
- [45] A. S. Zelenina, R. Quidant, and M. Nieto-Vesperinas, "Enhanced optical forces between coupled resonant metal nanoparticles," *Opt. Lett.*, vol. 32, pp. 1156–1158, 2007.
- [46] N. Lewinski, V. Colvin, and R. Drezek, "Cytotoxicity of nanoparticles," *Small*, vol. 4, pp. 26–49, Jan. 2008.
- [47] A. Pralle, M. Prummer, E. L. Florin, E. H. Stelzer, and J. K. Horber, "Three-dimensional high-resolution particle tracking for optical tweezers by forward scattered light," *Microsc. Res. Tech.*, vol. 44, pp. 378–386, Mar. 1, 1999.
- [48] K. Berg-Sørensen, L. Oddershede, E. L. Florin, and H. Flyvbjerg, "Unintended filtering in typical photo-diode detection system for optical tweezers," *J. Appl. Phys.*, vol. 93, pp. 3167–3176, 2003.
- [49] P. M. Hansen, I. M. Tolic-Nørrelykke, H. Flyvbjerg, and K. Berg-Sørensen, "Tweezercalib 2.0: Faster version of a MatLab package for precision calibration of optical tweezers," *Comp. Phys. Commun.*, vol. 174, pp. 518–520, 2006.
- [50] L. Bosanac, T. Aabo, P. M. Bendix, and L. B. Oddershede, "Efficient optical trapping and visualization of silver nanoparticles," *Nano Lett.*, vol. 8, pp. 1486–1491, May 2008.
- [51] A. Ashkin and J. P. Gordon, "Cooling and trapping of atoms by resonance radiation pressure," *Opt. Lett.*, vol. 4, pp. 161–163, Jun. 1 1979.
- [52] T. Čížmár, M. Mazilu, and K. Dholakia, "In situ wavefront correction and its application to micromanipulation," *Nat. Photon.*, vol. 4, pp. 388–394, 2010.
- [53] H. Ma, P. M. Bendix, and L. B. Oddershede, "Large-scale orientation dependent heating from a single irradiated gold nanorod," *Nano Lett.*, vol. 12, pp. 3954–3960, Aug. 8, 2012.
- [54] R. Weissleder, "A clearer vision for in vivo imaging," *Nat. Biotechnol.*, vol. 19, pp. 316–317, Apr. 2001.
- [55] P. J. Pauzauskis, A. Radenovic, E. Trepagnier, H. Shroff, P. Yang, and J. Liphardt, "Optical trapping and integration of semiconductor nanowire assemblies in water," *Nat. Mater.*, vol. 5, pp. 97–101, Feb. 2006.
- [56] Z. Yan, J. E. Jureller, J. Sweet, M. J. Guffey, M. Pelton, and N. F. Scherer, "Three-dimensional optical trapping and manipulation of single silver nanowires," *Nano Lett.*, vol. 12, pp. 5155–5161, Oct. 10, 2012.
- [57] Y. Shirasaki, G. J. Supran, M. G. Bawendi, and V. Bulović, "Emergence of colloidal quantum-dot light-emitting technologies," *Nat. Photon.*, vol. 7, pp. 13–23, 2013.
- [58] C. R. Head, E. Kammann, M. Zanella, L. Manna, and P. G. Lagoudakis, "Spinning nanorods—Active optical manipulation of semiconductor nanorods using polarised light," *Nanoscale*, vol. 4, pp. 3693–3697, Jun. 21, 2012.
- [59] L. Jauffred and L. B. Oddershede, "Two-photon quantum dot excitation during optical trapping," *Nano Lett.*, vol. 10, pp. 1927–1930, May 12, 2010.

- [60] L. Jauffred, A. C. Richardson, and L. B. Oddershede, "Three-dimensional optical control of individual quantum dots," *Nano Lett.*, vol. 8, pp. 3376–3380, Oct. 2008.
- [61] C. Nobile, V. A. Fonoberov, S. Kudera, A. D. Torre, A. Ruffino, G. Chilla, T. Kipp, D. Heitmann, L. Manna, R. Cingolani, A. A. Balandin, and R. Krahn, "Confined optical phonon modes in aligned nanorod arrays detected by resonant inelastic light scattering," *Nano Lett.*, vol. 7, pp. 476–479, Feb. 2007.
- [62] B. Hester, G. K. Campbell, C. Lopez-Mariscal, C. L. Filgueira, R. Huschka, N. J. Halas, and K. Helmerson, "Tunable optical tweezers for wavelength-dependent measurements," *Rev. Sci. Instrum.*, vol. 83, pp. 043114-1–043114-8, Apr. 2012.
- [63] P. K. Jain, K. S. Lee, I. H. El-Sayed, and M. A. El-Sayed, "Calculated absorption and scattering properties of gold nanoparticles of different size, shape, and composition: Applications in biological imaging and biomedicine," *J. Phys. Chem. B*, vol. 110, pp. 7238–7248, Apr. 13, 2006.
- [64] M. Sheik-Bahae, D. C. Hutchings, D. J. Hagan, and E. W. Stryland, "Dispersion of bound electronic nonlinear refraction in solids," *IEEE J. Quantum Electron.*, vol. 27, no. 6, pp. 1296–1309, Jun. 1991.
- [65] J. P. Barton and D. R. Alexander, "Fifth-order corrected electromagnetic field components for a fundamental Gaussian beam," *J. Appl. Phys.*, vol. 66, pp. 2800–2802, 1989.
- [66] P. M. Bendix, S. N. Reihani, and L. B. Oddershede, "Direct measurements of heating by electromagnetically trapped gold nanoparticles on supported lipid bilayers," *ACS Nano*, vol. 4, pp. 2256–2262, Apr. 27, 2010.
- [67] G. Baffou, M. P. Kreuzer, F. Kulzer, and R. Quidant, "Temperature mapping near plasmonic nanostructures using fluorescence polarization anisotropy," *Opt. Exp.*, vol. 17, pp. 3291–3298, Mar. 2, 2009.
- [68] E. J. Peterman, F. Gittes, and C. F. Schmidt, "Laser-induced heating in optical traps," *Biophys. J.*, vol. 84, pp. 1308–1316, Feb. 2003.
- [69] P. Haro-Gonzalez, W. T. Ramsay, L. Martinez Maestro, B. del Rosal, K. Santacruz-Gomez, C. Iglesias-de la Cruz Mdel, F. Sanz-Rodríguez, J. Y. Chooi, P. Rodriguez Sevilla, M. Bettinelli, D. Choudhury, A. K. Kar, J. García Solé, D. Jaque, and L. Paterson, "Quantum dot-based thermal spectroscopy and imaging of optically trapped microspheres and single cells," *Small*, vol. 9, pp. 2162–2170, Jun. 24, 2013.
- [70] H. H. Richardson, Z. N. Hickman, A. O. Govorov, A. C. Thomas, W. Zhang, and M. E. Kordesch, "Thermo-optical properties of gold nanoparticles embedded in ice: Characterization of heat generation and melting," *Nano Lett.*, vol. 6, pp. 783–788, Apr. 2006.
- [71] A. S. Urban, M. Fedoruk, M. R. Horton, J. O. Radler, F. D. Stefani, and J. Feldmann, "Controlled nanometric phase transitions of phospholipid membranes by plasmonic heating of single gold nanoparticles," *Nano Lett.*, vol. 9, pp. 2903–2908, Aug. 2009.
- [72] T. Baumgart, G. Hunt, E. R. Farkas, W. W. Webb, and G. W. Feigenson, "Fluorescence probe partitioning between Lo/Ld phases in lipid membranes," *Biochim. Biophys. Acta.*, vol. 1768, pp. 2182–2194, Sep. 2007.
- [73] V. Kotaidis, C. Dahmen, G. von Plessen, F. Springer, and A. Plech, "Excitation of nanoscale vapor bubbles at the surface of gold nanoparticles in water," *J. Chem. Phys.*, vol. 124, pp. 184702-1–184702-7, May 14, 2006.
- [74] A. Rohrbach and E. H. K. Stelzer, "Trapping forces, force constants, and potential depths for dielectric spheres in the presence of spherical aberrations," *Appl. Opt.*, vol. 41, pp. 2494–2507, May 1, 2002.
- [75] S. N. S. Reihani, S. A. Mir, A. R. Richardson, and L. B. Oddershede, "Significant improvement of optical traps by tuning standard water immersion objectives," *J. Opt.*, vol. 13, pp. 105301-1–105301-6, 2011.
- [76] E. L. Florin, A. Pralle, J. K. Horber, and E. H. Stelzer, "Photonic force microscope based on optical tweezers and two-photon excitation for biological applications," *J. Struct. Biol.*, vol. 119, pp. 202–211, Jul. 1997.
- [77] P. Zemanek, A. Jonas, L. Sramek, and M. Liska, "Optical trapping of nanoparticles and microparticles by a Gaussian standing wave," *Opt. Lett.*, vol. 24, pp. 1448–1450, Nov. 1, 1999.
- [78] L. Tong, V. D. Miljković, and M. Käll, "Optical manipulation of plasmonic nanoparticles using laser tweezers," *Proc. SPIE*, vol. 7762, pp. 77620O-1–77620O-8, 2010.
- [79] J. Prikulis, F. Svedberg, and M. Käll, "Optical spectroscopy of single trapped metal nanoparticles in solution," *Nano Lett.*, vol. 4, pp. 115–118, 2004.
- [80] J.-H. Zhou, L.-J. Qu, K. Yao, M.-C. Zhong, and Y.-M. Li, "Observing Nanometre Scale Particles with Light Scattering for Manipulation using optical tweezers," *Chin. Phys. Lett.*, vol. 25, pp. 329–331, 2008.
- [81] K. Pearce, F. Wang, and P. J. Reece, "Dark-field optical tweezers for nanometrology of metallic nanoparticles," *Opt. Exp.*, vol. 19, pp. 25559–25569, Dec. 5, 2011.
- [82] A. Ohlinger, A. Deak, A. A. Lutich, and J. Feldmann, "Optically trapped gold nanoparticle enables listening at the microscale," *Phys. Rev. Lett.*, vol. 108, pp. 018101-1–018101-5, 2012.
- [83] S. Duhr and D. Braun, "Thermophoretic depletion follows Boltzmann distribution," *Phys. Rev. Lett.*, vol. 96, pp. 168301-1–168301-4, Apr. 28, 2006.
- [84] M. J. Guffey and N. F. Scherer, "All-optical patterning of Au nanoparticles on surfaces using optical traps," *Nano Lett.*, vol. 10, pp. 4302–4308, Nov. 10, 2010.



Poul M. Bendix received the B.S. degree in mathematics and physics in 2002 and the Cand. Scient degree in physics in 2003 from Niels Bohr Institute (NBI) University of Copenhagen, Copenhagen, Denmark, and the Ph.D. degree in biophysics in 2007 following 6 months a visit at Harvard University, Cambridge, MA, USA. During his postdoc period from 2007 to 2011, he worked at the Nanoscience Center, University of Copenhagen, and at Stanford University, Stanford, CA, USA. Since 2013, he has been an Associate Professor at the NBI. His research

interests include interactions between light and nanoparticles with respect to both heating and trapping as well as biophysics of model membrane systems and mechanics of reconstituted cytoskeletal filaments. He received the Young Investigator Award in 2011 from the Villum Foundation.



Liselotte Jauffred received the B.S. degree in mathematics and physics in 2004 and the M.S. degree in physics in 2006 from the University of Copenhagen, Copenhagen, Denmark, and the Ph.D. degree from the Niels Bohr Institute (NBI) in biophysics in 2010. As a Postdoc, she has worked at the FOM Institute AMOLF, Amsterdam, Netherlands, and is currently a Postdoc at NBI. Her research includes interactions between light and quantum dots and she was the first to visualize and quantitate the forces exerted on an optically trapped quantum dot.



Kamilla Nørregaard received her B.S. degree in physics in 2009 and the Cand. Scient degree in physics in 2011 from the University of Copenhagen, Copenhagen, Denmark. Currently she is working toward the Ph.D. degree in biophysics under the guidance of P. M. Bendix and L. B. Oddershede. Her research interests include plasmonic heating and trapping of nanoparticles, nanoparticle mediated photothermal cancer therapy, and nanoparticle delivered gene therapy.



Lene B. Oddershede received the Cand. Scient degree in mathematics and physics and the Ph.D. degree in physics from University of Southern Denmark (SDU), Odense, Denmark, in 1995 and 1998, respectively. She visited the James Frank Institute, University of Chicago 1996–1997. In 1998, she became an Assistant Professor and constructed the optical tweezers laboratory at the Niels Bohr Institute (NBI), University of Copenhagen, Copenhagen, Denmark. In 2003, she was tenured and became an Associate Professor and group leader at the NBI. In 2003, she

received the Young Investigator Award from the Danish Optical Society and in 2011 the Silver Medal from the Danish Royal Academy of Sciences. Her research interests include the biophotonical and nanotoxicological properties of nanoparticles and their potential use in biological contexts. Also, she is interested in optical manipulation of biological specimen.